3D CFD-PBM Modeling of Industrial Fluidized Bed Polymerization Reactor for Polyethylene Production

Reis, Catarina [a,b]; Pornchai, Bumroongsri[b]; Geraldes, Vítor[a]

[a] Instituto Superior Técnico, Avenida Rovisco Pais, 1, 1049-001, Lisbon, Portugal
[b] Mahidol University, 999 Phuttamonthon 4 Road, Salaya, Nakhon Pathom 73170, Thailand

catarina.reis@tecnico.ulisboa.pt

Abstract

The present dissertation has the objective of developing a three-dimensional (3D) computational fluid dynamics (CFD) model integrated with the population balance model (PBM) and study the polyethylene (PE) particle flow patterns considering particle growth in industrial-scale fluidized bed reactor (FBR), utilizing ANSYS Fluent software.

A CFD model was developed to study the cold-flow behavior of PE particles in a pilot-scale FBR, where the polymerization reaction was not considered, and the particle flow behavior and the bed pressure drop of PE particles were predicted.

In order to validate the model, two different velocities were simulated: 3.3 m/s and 5.7 m/s (Re=870 and Re=1520, respectively). The predicted results reveal an acceptable agreement with the observed experimental data obtained from the faculty laboratory's pilot-scale fluidization unit and theoretical values regarding pressure drop. Comparing the theoretical value (5.89 mbar) with the experimental value (7 mbar) and the simulation result (5.91 mbar), there is an error of 18.9% and 0.3%, respectively.

The developed model was coupled with PBM and performed in an industrial-scale FBR at 0.38 m/s (Re=770). The model is able to represent the actual behavior of real mixture with reasonable accuracy with a 1.7% error between simulation result and theoretical value of pressure drop. The simulation results show that through time, the average particle size increase with a particle growth rate of 1.62 μm/s, obtaining a final average diameter of 545.1 μm, from an initial average diameter of 200 μm.

Hence, the 3D CFD-PBM coupled model can be used as a reliable tool for analyzing and improving the design and operation of the gas phase polymerization FBRs.

keywords: Polyethylene, Computational fluid dynamics, Population balance model, Fluidized bed reactor, Fluidization

1. INTRODUCTION

Polyethylene (PE) is a thermoplastic polymer with a variable crystalline structure, and it has the simplest basic structure of any polymer. Polymerizing the gas ethylene, C_2H_4, used as a monomer, is obtained PE. [1] Due to the great versatility of the physical and chemical properties of PE, and to the fact that it can be produced using various technologies with a wide range of possible uses, PE is one of the most widely produced plastics in the world.

The global production capacity was around 113 million metric tonnes in 2017, and the global production capacity increase is expected, being approximately 133 million metric tons in 2022 with an annual growth rate of 3%. [2]

Commercially, PE is produced from ethylene and was accidentally discovered in 1933, while researching ethylene reactions at high temperatures and pressures by Imperial Chemical Company. In 1992 was introduced the latest significant new technology, the single-site catalyzed or metallocene-catalyzed polyethylene resins, resulting in the commercial introduction of several new polyethylenes. [1] According to Figure 1, it is possible to observe the main innovations in PE production over time.

PE production techniques improvement and development have been the subject of several studies with the essential objective of reducing manufacturing cost. [4] Two ways can be followed to obtain PE. The first way consists of the high pressure polymerization that produces LDPE.

The second way consists of the low pressure catalytic polymerization producing LLDPE and HDPE. The second way can be used three types of catalyst, Ziegler/Natta, Cr/Mo oxide, and Metallocene, in three different processes, solution, slurry, and gas phase processes. This work focuses only on the production of PE in gas-phase.

According to this process, the polymerization reaction takes place in a fluidized bed reactor (FBR). PE production process widely uses FBR due to its several advantages such as high heat and mass transfer rates,

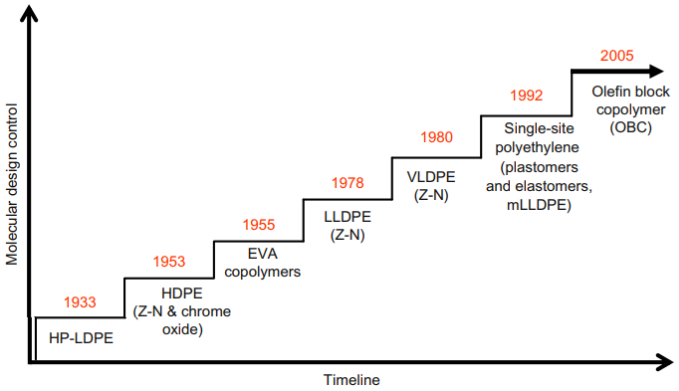

Figure 1 - Polyethylene innovations versus time. Adapted from [3]

simple construction, considerable particle mixing rate, and capability of continuous transport. [5]

In this reactor, small catalyst particles are continuously fed into the reactor that reacts with the incoming gaseous monomer to produce polymer particles with a broad size distribution that directly affect the quality of the final product, mixing/segregation, and hydrodynamic parameters.

Ethylene polymerization is a highly exothermic reaction, and the produced heat must be removed as soon as possible to keep the temperature constant in the reactor. Otherwise, it may lead to hot spots or lump formation.

Regarding the chemical reaction efficiencies, transfer properties, and energy consumptions always depend on the reactor temperature field and the solid mixing/contacting state, which relies on the particle flow patterns in FBRs.

Thus, an efficient reacting gas and solid particle flow and mixing are of prime importance for FBR operation since that an improper fluidization can lead to an ineffective reaction, heat/ mass transfer, inability to

maintain uniform distribution of temperature, and accumulation of large polymer particles.

To operate FBR more effectively, improve design and scale-up of polydispersed gas phase fluidized bed process is crucial to obtain a fundamental understanding of the gas-solid two-phase flow behaviors considering the temperature fields in the FBR, and a precise prediction of the particles size distribution (PSD).

In this respect, advanced computational methods and computer programming have made it possible for computational fluid dynamics (CFD) to become an efficient technique to predict the macroscopic fluid dynamics, transport phenomena in a gas-solid fluidized bed, and understand the influence of the fluid dynamics on the performance of chemical reactors.

Lately, the CFD models have been employed to analyze the scale-up performance and are an important engineering tool for FBRs at industrial scale predicting their flows.

The polymerization kinetics, particle growth, aggregation, and breakage of particles influence the PSD, so, the population balance model (PBM) should be coupled with the CFD model since PBM is used to compute the size distribution of the dispersed phase [5].

Several articles have been dedicated to FBR for PE production and its modeling.

Regarding pilot-scale reactors, the last articles studied the effect of the method of moments with a 2D CFD-PBM model considering particle growth and aggregation [12], and the temperature field and particle flow patterns with a 3D CFD-PBM model [6] by Yao et al. and Che et al., respectively.

On the other hand, for industrial-scale reactors, Akbari et al. developed a 2D CFD-PBM model for hydrodynamic and particle growth simulation [5], and hydrodynamics and mixing/segregation simulation [9].

This dissertation aims to develop a 3D CFD-PBM model for hydrodynamic and particle growth simulation to an industrial-scale FBR for PE production.

Thus, the main objectives are to 1) develop a CFD model to predict the cold-flow behavior of PE particles in a pilot-scale fluidization unit, 2) perform the CFD model and validate it with experimental data and empirical equations, and 3) develop and perform a CFD model coupled with PBM in an industrial-scale FBR.

1.1 POLYETHYLENE PRODUCTION

The catalyst, monomer, and other process fluids are fed to the reactor train. Figure 2 shows a general illustration of the basic blocks of an industrial polymerization unit.

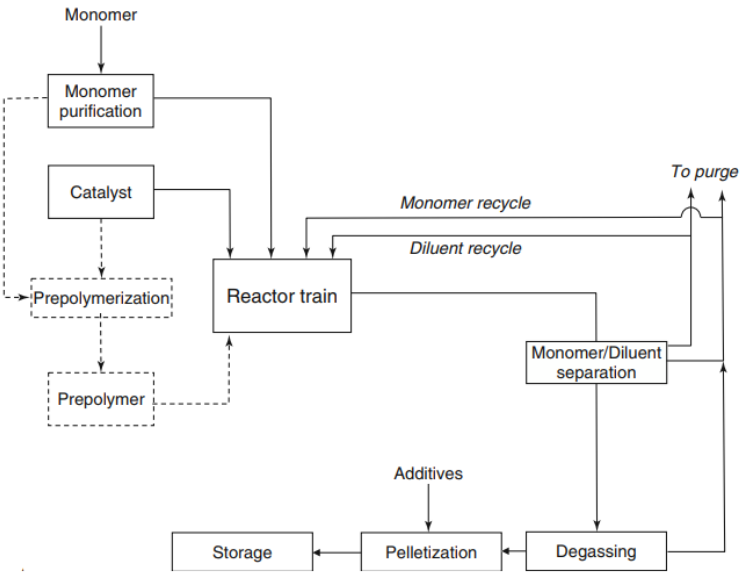

Figure 2 – General schema of polyolefin production unit using Z-N catalysts. Adapted from [8]

Typically, in slurry conditions, the use of a prepolymerization step is necessary in order to avoid loss of control over the reaction and the morphology due to the high reaction rates during the fragmentation step. This procedure helps to increase the activity of the catalyst in the main reactor and allows us to produce polymer at a reasonable rate.

Heat and mass transfer limitations are reduced to manageable levels or eliminated at all since those particles are grown to a large enough size. [8] Hot spots are more likely to occur in smaller particles, and the reaction is slower since the surface area is smaller. After exiting the reactor, there is the separation of the diluent, if used, and subsequent recycling of the monomer and diluent to the reactor train.

1.2 GAS-PHASE PROCESS

This process is used in a **low pressure** catalytic polymerization. The operating pressure range is between 10 to 80 bar. The polymerization reaction takes place in a FBR. No solvent is used, the ethylene monomer in the gaseous state is blown into the reactor, and the supported catalyst is continuously fed above the distributor plate. As the PE molecule is polymerized, it precipitates as a solid dispersed, as a fluid bed in the reactor. The gas circulates through the polymerizing fluidized bed, and the reactor temperature must be kept below 115ºC to prevent the solid melting. The injection of a cooled gas stream and inert monomer removes the heat of reaction. The main catalysts used are Ziegler-Natta, Chrome oxide based, and Metallocene. Although gas species has poor thermal characteristics, some special steps are taken to enhance heat transfer and to keep gas-phase reactors economically competitive in terms of productivity. This step can be an injection of small amounts of liquid components below their dew points or the use of inert gas-phase compounds with higher heat capacities.

This work focuses only on the gas-phase process with a Z-N catalyst.

1.3 FLUIDIZED BED REACTOR [8]

FBR's are the only type of reactors used in gas-phase processes because they have the best heat removal capacity. [8]

The FBR is essentially an empty cylinder with a distributor plate at the bottom and divides into three zones: reaction zone, freeboard zone, and disengagement zone.

A schema of an FBR is shown in Figure 3.

The reaction zone, with a height of 10-15 m, locates immediately above the distribution plate and below the freeboard zone. It is where the polymerization takes place. The injection of catalyst is above the distributor plate, and product particles are also withdrawn at similar bed height. The catalyst injection might be done using propane than nitrogen to avoid hot spots in the feed zone because propane has a higher heat capacity. The central role of the distributor plate is to distribute the components in the powder bed in a proper manner.

The holes in the plate allow the gases to pass and orient them in order to promote fluidization. The configuration of the holes must prevent particle deposition on the plate and blockage of gas flow. With a reduced gas flow rate into the reactor, the heat removal capacity decreases, resulting in the polymer meltdown inside the reactor.

Superficial gas velocity is between 0,5-1 m/s, and the relative gas-particle velocity is 2-8 times the minimum fluidization velocity. In order to achieve such high flow rates, typically uses recycle ratios up to 50, with lower per pass conversion, 2-30%. However, conversions are usually higher than 95%.

After the reaction zone, the unreacted gases with fine particles enter into the disengaging zone that facilitates the separation of solids from the gas. The recycled free of solids is recovered at the top of the bed.

Sometimes, the recycled stream can include condensable material to improve heat removal capacity. At the freeboard zone, the void fraction is near one, and generally, particle velocity is below minimum fluidization velocity. Some particles will fall back into the bed. The particles small enough get blown through the freeboard zone. To minimize the amount of particles passing through the freeboard zone, the diameter in the

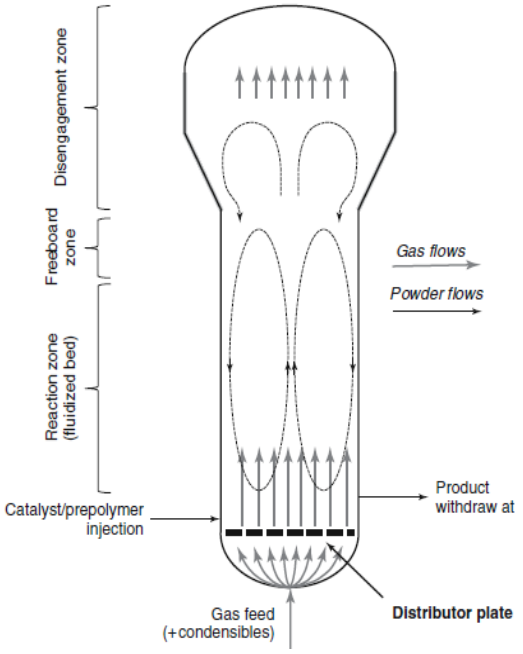

Figure 3- Schematic diagram of an industrial fluidized-bed polyethylene reactor. [8]

disengagement zone is increased so that the superficial gas velocity decreases.

The minimum fluidization velocity must be guaranteed, so there is no collapse of the fluidized bed, but at the same time, a high superficial velocity can pneumatically transport the particles. On another hand, there are some limitations on the increase of the gas flow rate since the bigger the rate, the smaller the conversion for each pass, and the recycle ratios increase.

Depending on the velocity, different fluidization regimes may occur.The FBRs used in PE production tend to operate in a bubbling regime.

The pressure drop in FBRs is one of the crucial parameters in the proper scale-up and design of FBRs. When the particles in FBRs are fluidized, the pressure gradient can be calculated according to the following classical equations [12],

$$\Delta P_s = (\rho_s - \rho_g)(1-\varepsilon)gL \quad (1)$$

$$\Delta P_g = \rho_g \varepsilon g L \quad (2)$$

1.4 KINETIC MODEL [6] [9]

Ethylene polymerization kinetics using Ziegler–Natta catalysts is relatively complicated, and the chemical kinetic scheme comprises a series of elementary reactions.

In order to describe the kinetics of ethylene polymerization in CFD modeling, a kinetics model containing the mainly elementary chain propagation reaction is adopted and the polymerization rate R_p can be calculated as

$$R_p = k_p[C][M] \quad (3)$$

where $[M]$ is the concentration of monomer, $[C]$ is the concentration of catalyst active site and k_p is the propagation rate defined as,

$$k_p = k_{p0} exp\left(-\frac{E_a}{RT}\right) \quad (4)$$

The heat produced from polymerization reaction is expressed as

$$\Delta Q_{rs\alpha} = R_p \Delta H \quad (5)$$

1.5 COMPUTATIONAL FLUID DYNAMICS

Computational fluid dynamics (CFD) is a method of predicting fluid flow, heat and mass transfer, chemical reaction, and other related phenomena by numerically solving the equations that characterize these phenomena.

I. EULERIAN-EULERIAN TWO FLUIDS [9] [30]

The Eulerian-Eulerian approach was used to describe the gas-solid two flows in this work. The gas phase is considered as the primary phase, whereas the solid phase is considered as the secondary or dispersed phase.

The continuity equations of gas and solid phases can be written as

$$\frac{\partial}{\partial t}(\alpha_g \rho_g) + \nabla(\alpha_g \rho_g v_g) = -\dot{m}_{gs} \quad (6)$$

$$\frac{\partial}{\partial t}(\alpha_s \rho_s) + \nabla(\alpha_s \rho_s v_s) = \dot{m}_{gs} \quad (7)$$

where the mass transfer from the gas phase to the solid phase can be calculated as

$$\dot{m}_{gs} = \frac{1}{2}\pi \rho_s G_{m2} \quad (8)$$

The momentum balance equation for the gas phase is expressed as:

$$\frac{\partial}{\partial t}\left(\alpha_g \rho_g v_g\right) + \nabla\left(\alpha_g \rho_g v_g v_g\right) = -\alpha_g \nabla p + \nabla \cdot \bar{\bar{\tau}}_g + K_{gs}(v_s - v_g) + \alpha_g \rho_g g - \dot{m}_{gs} v_g \quad (9)$$

and the shear stress of gas phase $\bar{\bar{\tau}}_g$ can be calculated as:

$$\bar{\bar{\tau}}_g = \alpha_g \mu_g (\nabla \cdot v_g + \nabla \cdot v_g{}^T) \quad (10)$$

The momentum balance equation for solid-phase is expressed as:

$$\frac{\partial}{\partial t}(\alpha_s \rho_s v_s) + \nabla(\alpha_s \rho_s v_s v_s) = -\alpha_s \nabla p + \nabla \cdot \bar{\bar{\tau}}_s - \nabla p_s + K_{gs}(v_g - v_s) + \alpha_s \rho_s g - \dot{m}_{gs} v_s \quad (11)$$

and the shear stress of solid phase $\bar{\bar{\tau}}_s$ can be calculated as:

$$\bar{\bar{\tau}}_s = \alpha_s \mu_s (\nabla \cdot v_s + \nabla \cdot v_s{}^T) + \alpha_s \left(\lambda_s - \frac{2}{3}\mu_s\right) \nabla \cdot v_s \cdot \bar{\bar{I}} \quad (12)$$

The energy balance equations for gas and solid phases are described as (8) and (9), respectively.

$$\frac{\partial}{\partial t}(\alpha_g \rho_g h_g) + \nabla(\alpha_g \rho_g v_g h_g) = -\alpha_g \frac{\partial p_g}{\partial t} + \bar{\bar{\tau}}_g : \nabla v_g - \nabla \cdot q_g + \sum_{p=1}^{n}(Q_{gs} + \dot{m}_{gs} h_{gs} - \dot{m}_{sg} h_{sg}) \quad (13)$$

$$\frac{\partial}{\partial t}(\alpha_s \rho_s h_s) + \nabla(\alpha_s \rho_s v_s h_s) = -\alpha_s \frac{\partial p_s}{\partial t} + \bar{\bar{\tau}}_s : \nabla v_s - \nabla \cdot q_s + \sum_{p=1}^{n}(Q_{sg} + \dot{m}_{sg} h_{sg} - \dot{m}_{gs} h_{gs}) + \Delta Q_{rs\alpha} \quad (14)$$

where the specific enthalpy of gas phase, h_g, and the specific enthalpy of solid phase, h_s, can be calculated as

$$h_i = \int_{T\,ref}^{T} C_{P,i}\, dT_i \qquad i = g \text{ or } s \quad (15)$$

The heat flux of the gas phase q_g and the heat flux of the solid phase q_s can be calculated as

$$q_i = -\alpha_i \kappa_i \nabla T_i \qquad i = g \text{ or } s \quad (16)$$

II. KINETIC THEORY OF GRANULAR FLOW [9] [12]

KTGF is used to describe the rheology of the solid phase and some properties such as the solid viscosity, solid pressure, and granular temperature.

The kinetic theory concepts used in this work were derived by Lun et al. [13] as follows

$$p_s = \alpha_s \rho_s \Theta_s (1 + 2 g_0 \alpha_s (1 + e_s)) \quad (17)$$

$$\lambda_s = \frac{4}{3} {\alpha_s}^2 \rho_s d_s g_0 (1 + e_s) \sqrt{\frac{\Theta_s}{\pi}} \quad (18)$$

where

$$g_0 = \frac{1}{1 - \left(\frac{\alpha_s}{\alpha_{s\,max}}\right)^{1/3}} \quad (19)$$

$$\Theta_s = \frac{1}{3} \langle v'_s \rangle^2 \quad (20)$$

A balance of the granular energy associated with particle velocity fluctuations is required to supplement the continuity and momentum balance for both phases [14],

$$\frac{3}{2}\left[\frac{\partial}{\partial t}(\rho_s \alpha_s \Theta_s) + \nabla(\rho_s \alpha_s \Theta_s v_s)\right] = \left(-p_s \bar{\bar{I}} + \bar{\bar{\tau}}_s\right) : \nabla v_s - \nabla(k_{\Theta s} \nabla \Theta_s) - \gamma_{\Theta_s} - \Phi_{gs} \quad (21)$$

The diffusion coefficient for granular energy, k_{gs}, is given by Syamlal et al. [35] as

$$k_{gs} = \frac{15 \rho_s d_s \alpha_s \sqrt{\Theta_s \pi}}{4(41 - 33\eta)}\left[1 + \frac{12}{5}\eta^2 (4\eta - 3)\alpha_s g_0 + \frac{16}{15\pi}(41 - 33\eta)\eta \alpha_s g_0\right] \quad (22)$$

with

$$\eta = \frac{1}{2}(1 + e_s) \quad (23)$$

The collision dissipation of energy γ_{Θ_s} is given by Lun et al. [13] as

$$\gamma_{\Theta_s} = \frac{12(1 - {e_s}^2)}{d_s \sqrt{\pi}} \rho_s {\alpha_s}^2 {\Theta_s}^{1,5} \quad (24)$$

$$\Phi_{gs} = -3 K_{gs} \Theta_s \quad (25)$$

In the transport equation for the granular temperature, the convection and diffusion can be neglected assuming that the granular energy is at steady-state and dissipated locally. Thereby, the simplified transport equation for the granular temperature is as follow

$$0 = \left(-p_s \bar{\bar{I}} + \bar{\bar{\tau}}_s\right) : \nabla v_s - \gamma_{\Theta_s} - 3 K_{gs} \Theta_s \quad (26)$$

The solid shear viscosity μ_s can be calculated as

$$\mu_s = \mu_{s,col} + \mu_{s,kin} + \mu_{s,fr} \quad (27)$$

$$\mu_{s,col} = \frac{4}{5}\alpha_s \rho_s d_s g_0 (1 + e_s)\sqrt{\frac{\Theta_s}{\pi}} \quad (28)$$

$$\mu_{s,kin} = \frac{10 \rho_s d_s \sqrt{\Theta_s \pi}}{96 \alpha_s (1 + e_s) g_0}\left[1 + \frac{4}{5}(1 + e_s)\alpha_s g_0\right]^2 \quad (29)$$

$$\mu_{s,fr} = \frac{p_s \sin\theta}{2\sqrt{I_{2D}}} \quad (30)$$

III. TURBULENCE MODEL [10]

A turbulence model is a computational procedure that allows to close the system of mean flow equations and the calculation of the mean flow without first calculating the full time-dependent flow field.

The standard κ - ε model was employed in this work.The transport equations for the turbulence kinetic energy κ and the turbulence dissipation rate ε can be written as

$$\frac{\partial}{\partial t}(\rho_m \kappa) + \nabla \cdot (\rho_m \kappa \vec{v}_m) = \nabla \cdot \left(\mu + \frac{\mu_{t,m}}{\sigma_\kappa}\nabla \kappa\right) + G_{\kappa,m} - \rho_m \varepsilon \quad (31)$$

$$\frac{\partial}{\partial t}(\rho_m \varepsilon) + \nabla \cdot (\rho_m \varepsilon \vec{v}_m) = \nabla \cdot \left(\mu + \frac{\mu_{t,m}}{\sigma_\varepsilon}\nabla \varepsilon\right) + \frac{\varepsilon}{\kappa}\left(C_{1\varepsilon} G_{\kappa,m} - C_{2\varepsilon} \rho_m \varepsilon\right) \quad (32)$$

where

$$\rho_m = \alpha_s \rho_s + \alpha_g \rho_g \quad (33)$$

$$\vec{v}_m = \frac{\alpha_s \rho_s \vec{v}_m + \alpha_g \rho_g \vec{v}_m}{\alpha_s \rho_s + \alpha_g \rho_g} \quad (34)$$

$$\mu_{t,m} = \rho_m C_\mu \frac{\kappa^2}{\varepsilon} \quad (35)$$

$$G_{\kappa,m} = \mu_{t,m}\left(\nabla \vec{v}_m + (\nabla \vec{v}_m)^T\right) : \nabla \vec{v}_m \quad (36)$$

with. $C_{1\varepsilon} = 1{,}44$, $C_{2\varepsilon} = 1{,}92$ and $C_\mu = 0{,}09$ as the turbulent model coefficients.

IV. DRAG FORCE MODEL [9] [10]

In the Eulerian-Eulerian model, the transfer of forces between the gas and particle phases is done by the drag force.

The drag force model has a critical effect on the hydrodynamics of FBRs, and several models are used to calculate the drag coefficient.

In this work, the Gidaspow model describes the momentum transfer between the gas and solid phase. [39]

$$K_{sg} = \frac{3}{4} C_D \frac{\alpha_s \alpha_g \rho_g |v_s - v_g|}{d_s} \alpha_g^{-2{,}65}, \quad \alpha_g > 0{,}8 \quad (37)$$

$$K_{sg} = 150 \frac{\alpha_s (1 - \alpha_g)\mu_g}{\alpha_g {d_s}^2} + \frac{7}{4}\frac{\alpha_s \rho_g |v_s - v_g|}{d_s}, \quad \alpha_g \le 0{,}8 \quad (38)$$

where

$$C_D = \frac{24}{\alpha_g Re_s}\left[1 + \left(\frac{3}{20}\alpha_g Re_s\right)^{0{,}687}\right], \quad Re_s \le 1000 \quad (39)$$

$$C_D = 0{,}44 \ , \quad Re_s > 1000 \quad (40)$$

The Reynolds number Re_s can be calculated as

$$Re_s = \frac{\rho_g d_s |v_s - v_g|}{\mu_g} \quad (41)$$

V. HEAT TRANSFER COEFFICIENT [11]

The rate of energy transfer between gas and solid phases are expressed as follows:

$$Q_{gs} = h_{gs}(T_s - T_g) \quad (42)$$

$$h_{gs} = \frac{6 \kappa_g \alpha_g \alpha_s Nu_s}{{d_s}^2} \quad (43)$$

For the solid particles placed in a continuously moving gas phase, the Ranz–Marshall correlation for the dimensionless heat transfer coefficients is applied in this work to determine the Nusselt number as follow,

$$Nu_s = 2{,}0 + 0{,}6 {Re_s}^{1/2} Pr^{1/3} \quad (44)$$

$$Pr = \frac{C_{P,g}\,\mu_g}{k_g} \quad (45)$$

1.6 POPULATION BALANCE MODEL [5][9][11]

The real heterogeneous polymerization systems in FBR are polydisperse.

In the first stage of the polymerization, the catalyst breaks down into many smaller particles, which are quickly encapsulated by the growing semi-crystalline polymer. During their residence in the reactor, the size of the catalyst particles grows due to polymerization. The aggregation of particles that occurs inside the reactor also contributes to the growth of

particles. However, the particle size might decrease due to the particle attrition or breakage.

The reaction system is considered as a gas-solid two-phase system, and the solid phase can be characterized by particle-size distribution (PSD) that is directly related to particle growth, aggregation, and breakage dynamics, as shown in Figure 4.

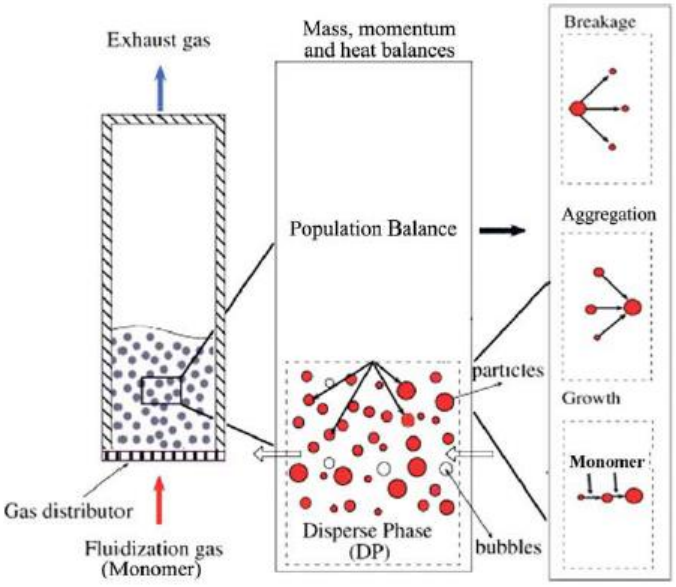

Figure 4 - The evolution of particle-size distribution in the fluidized-bed olefin polymerization reactor. [15]

The polydispersity can enlarge considering all these aspects.

This PSD also can directly affect the quality of the product, mixing, and hydrodynamic parameters. Thus, to operate FBR more effectively is necessary to obtain a fundamental understanding and describe the gas-solid two-phase flow behaviors of a polymerization system with solid PSD. The CFD model has to be solved together with the PBM.

A general form of PBM based on the length number density function (NDF) can be expressed as

$$\frac{\partial n(L;\vec{x},t)}{\partial t}+\nabla\cdot[\vec{u}n(L;\vec{x},t)]=S(L;\vec{x},t)=-\frac{\partial}{\partial L}[G(L)n(L;\vec{x},t)]$$
$$+B_{ag}(L;\vec{x},t)-D_{ag}(L;\vec{x},t)+B_{br}(L;\vec{x},t)-D_{br}(L;\vec{x},t) \quad (46)$$

where $n(L;\vec{x},t)$is the NDF with particle size, L, as the internal coordinate, $\vec{u}$ is the particle velocity vector, $S(L;\vec{x},t)$ is the source term representing the particle growth, aggregation, and breakage. $G(L)n(L;\vec{x},t)$ is the particle flux for the growth rate, $B_{br}(L;\vec{x},t)$ and $D_{br}(L;\vec{x},t)$ are the birth and death rates, respectively, of the particles to breakage, and $B_{ag}(L;\vec{x},t)$ and $D_{ag}(L;\vec{x},t)$ are the birth and death rates of particles, respectively, for aggregation.

I. QUADRATURE METHOD OF MOMENT

In order to track the evolution of the particle size by solving a system of differential equations in lower order moments, the QMOM is applied in this work.

The moments of the particle size distribution (PSD) are determined as

$$\mathrm{m_{kk}}(\vec{x},\mathrm{t})=\int_0^\infty \mathrm{n}(\mathrm{L};\vec{x},\mathrm{t})\mathrm{L^{kk}}\,\mathrm{dL}, \quad \mathrm{kk}=0,1,\ldots,2\mathrm{N}- \quad (47)$$

where N is the order of quadrature approximation, kk is the specified number of moments.

The Sauter diameter, L_{32}, is used to calculate the mean particle size and can be written as

$$\mathrm{L_{32}}=\frac{\mathrm{m_3}}{\mathrm{m_2}} \quad (48)$$

Applying the moment transformation into the population balance equation, the transport equation for the kk^{th} moment can be written as

$$\frac{\partial m_{kk}}{\partial t}+\nabla\cdot[\vec{u}m_{kk}]=-\int_0^\infty kkL^{kk-1}G(L)n(L;\vec{x},t)dL+B_{ag,kk}(L;\vec{x},t)$$
$$-D_{ag,kk}(L;\vec{x},t)+B_{br,kk}(L;\vec{x},t)-D_{br,kk}(L;\vec{x},t) \quad (49)$$

where

$$\mathrm{B_{ag,kk}}=\frac{1}{2}\int_0^\infty \mathrm{n}(\lambda;\vec{x},\mathrm{t})\int_0^\infty \beta(\lambda,\mathrm{L})(\lambda^3+\mathrm{L}^3)^{\frac{\mathrm{kk}}{3}}\mathrm{n}(\lambda;\vec{x},\mathrm{t})\,\mathrm{dLd}\lambda \quad (50)$$

$$\mathrm{D_{ag,kk}}=\int_0^\infty \mathrm{L^{kk}n}(\mathrm{L};\vec{x},\mathrm{t})\int_0^\infty \beta(\lambda,\mathrm{L})\mathrm{n}(\lambda;\vec{x},\mathrm{t})\,\mathrm{dLd}\lambda \quad (51)$$

$$\mathrm{B_{br,kk}}=\int_0^\infty \mathrm{L^{kk}}\int_0^\infty \mathrm{a}(\lambda)\mathrm{b}(\mathrm{L}|\lambda)\mathrm{n}(\lambda;\vec{x},\mathrm{t})\,\mathrm{dLd}\lambda \quad (52)$$

$$\mathrm{D_{br,kk}}=\int_0^\infty \mathrm{L^{kk}a}(\mathrm{L})\mathrm{n}(\mathrm{L};\vec{x},\mathrm{t})\,\mathrm{dL} \quad (53)$$

where $\beta(\lambda,\mathrm{L})$ is the aggregation kernel representing the rate coefficient for aggregation of two particles with lengths L and λ. $\mathrm{a}(\mathrm{L})$ is the breakage kernel representing the rate coefficient for breakage of a particle of size L. $b(\mathrm{L}|\lambda)$ is the fragment distribution function for the breakage of a particle with length L.

The QMOM based on the quadrature approximation can be written as

$$\mathrm{m_{kk}}=\int_0^\infty \mathrm{n}(\mathrm{L};\vec{x},\mathrm{t})\,\mathrm{L^{kk}}\,\mathrm{dL}\approx\sum_{\mathrm{i}=1}^{\mathrm{N}}\mathrm{w_i}\mathrm{L_i}^{\mathrm{kk}}, \quad \mathrm{kk}=0,1,\ldots,2\mathrm{N}-1 \quad (54)$$

where the weights, w_i, and abscissas, L_i, are computed through the product-difference algorithm from the lower order moments.

Applying the quadrature approximation, the transport equation for the kk^{th} moment can be written as

$$\frac{\partial m_{kk}}{\partial t}+\nabla\cdot[\vec{u}m_{kk}]=kk\sum_{i=1}^{N}L_i^{kk-1}G(L_i)w_i+\frac{1}{2}\sum_{i=1}^{N}w_i\sum_{j=1}^{N}w_j$$
$$\left(L_i^3+L_j^3\right)^{\frac{kk}{3}}\beta\left(L_i,L_j\right)-\sum_{i=1}^{N}L_i^{kk}w_i\sum_{j=1}^{N}w_j\,\beta\left(L_i,L_j\right)+$$
$$\sum_{i=1}^{N}w_i\int_0^\infty L_{kk}a\,(L_i)b(L|L_i)\,dL-\sum_{i=1}^{N}L_i^{kk}\,w_ia(L_i) \quad (55)$$

This equation can be solved following the evolution of w_i, and L_i.

Considering that in this work the effect of aggregation and breakage was not considered, the details of the aggregation kernel, the breakage kernel, and the fragment distribution function can be found in Che et al. (2015) [18].

II. PARTICLE GROWTH RATE

Polymer formation on the surface of the catalyst pores begins as soon as the reactant species reach the active sites of the catalyst and react. The polymer particle starts growing by expansion.

The local value of PE particle growth rate can be expressed in terms of the overall particle polymerization rate, and it can be calculated as follows,

$$\mathrm{G(L_i)}=\frac{\mathrm{d(L_i)}}{\mathrm{dt}}=\frac{\mathrm{R_p{L_0}^3}}{3\rho_\mathrm{s}{\mathrm{L_i}}^2} \quad (56)$$

2. NUMERICAL METHODS

2.1 CFD MODEL - PILOT-SCALE FLUIDIZATION UNIT

A 3D CFD model was developed to study the cold-flow behavior of PE particles in a pilot-scale fluidization unit. The software ANSYS Fluent 16.0 was used to develop the model.

The population balance, polymerization heat, and polymerization kinetics are not considered. In order to get the right prediction of the particle flow behavior and the bed pressure drop of PE particles were defined the geometry, mesh, and setup simulation data for the pilot-scale fluidization unit.

The pilot-scale fluidization unit geometry has been designed according to the equipment instruction manual provided by the manufacturer. The shape of the unit is the pilot-scale of an industrial FBR for PE production.

Three different meshes were generated and subjected to sensitivity analysis in order to investigate the adequate number of computational cells to predict the flow behavior.

According to the sensitivity analysis of the nodes number of the mesh, the 118 557 nodes mesh was chosen to perform the simulation, Figure 5. The average pressure drop for the simulation with 118 557 nodes mesh is 5.91 mbar, with an associated error of 0.34% compared to the theoretical value (5.89 mbar). The theoretical value was obtained from the classical equation (1) and (2).

The simulation conditions and the properties of gas and solid phases are displayed in Table 1 and Table 2, respectively.

Table 1- Boundary conditions and model parameters for CFD model simulation in a pilot-scale fluidization unit.

Description	Values
Granular viscosity	Gidspow
Granular bulk viscosity	Lun et al.
Frictional viscosity	Schaeffer
Angle of internal friction	30º
Granular temperature	Algebraic
Drag law	Gidspow
Coefficient of restitution for particle-particle collisions	0.9
Inlet boundary conditions	Velocity inlet
Outlet boundary conditions	Pressure outlet
Wall boundary conditions	No slip for air, specularity coefficient 0 for solid phase
Initial bed height	0.1 m
Initial volume fraction of solid phase	0.63
Operating pressure	1 atm
Inlet gas velocity	3.3 m/s
Turbulent kinetic energy	0.000687 m^2/s^2
Turbulent dissipation rate	0.000128 m^2/s^3
Convergence criteria	0.001
Time step	0.001 s

The velocity used in the simulation and the experiment with the pilot-scale fluidization unit was $4u_{mf}$, 3.3 m/s.

Table 2- Physical properties of gas and solid phases for CFD model simulation in a pilot-scale fluidization unit

Physical properties	Air	Solids
Density, kg/m³	1.225	953
Viscosity, kg/(m·s)	$1.08 \cdot 10^{-5}$	-
Diameter, µm	-	2500

2.2 CFD-PBM COUPLED MODEL - INDUSTRIAL-SCALE FBR

The previous 3D CFD validated model in 3. EXPERIMENTAL METHODS is coupled with PBM. This new model is developed to study the flow behavior of PE particles and to track the changes in PSD in an industrial-scale FBR. It is considered the population balance, polymerization heat, and polymerization kinetics.

The software ANSYS Fluent 16.0 was used to develop the model where the geometry and the mesh of the industrial-scale FBR were defined for more ahead predict the particle flow behavior, and the bed pressure drop of PE particles.

The industrial-scale FBR geometry has been designed according to two articles that provide the dimensions of an industrial-scale FBR [9][5]. In the articles used to support geometry drawing, not all the dimensions required to draw geometry are defined. The remaining dimensions were defined by similarity ratios between pilot-scale and industrial-scale geometry.

It is essential to get a suitable number of cells that are adequate to predict the hydrodynamics in the FBR and provide grid-independent results. Three different meshes were generated and subjected to sensitivity analysis in order to investigate the adequate number of computational cells to predict the flow behavior.

According to the sensitivity analysis of the nodes number of the mesh**,** the 309 551 nodes mesh was chosen to perform the simulation, Figure 6.

The average pressure drop for the simulation with 309 551 nodes mesh is 0.4085 bar, with an associated error of 1.65% compared to the theoretical value (0.4153 bar). The theoretical value was obtained from the classical equation (1) and (2).

The particle growth rate equations, polymerization heat, and polymerization kinetics, are all defined using User Defined Functions (UDF).

The basic equations for CFD modeling are taken from the previous model used for the pilot-scale fluidization unit. The gas phase properties are not the same since that now, it is considered the real mixture present in the industry and that it is used to produce PE.

The simulation conditions, the properties of gas and solid phases, kinetic variables values, boundary conditions and model parameters are displayed in Table 3, Table 4, and Table 5, respectively.

Table 3- Physical properties of gas and solid phases for CFD-PBM model simulation in an industrial-scale FBR [5][9]

Physical properties	Gas	Solids
Density, kg/m³	20	850
Viscosity, kg/(m·s)	$1.2 \cdot 10^{-5}$	-
Heat capacity, J/(kg· K)	1817	2104
Thermal conductivity (W/(m· K)	0.023065	0.084
Temperature (K)	313	361

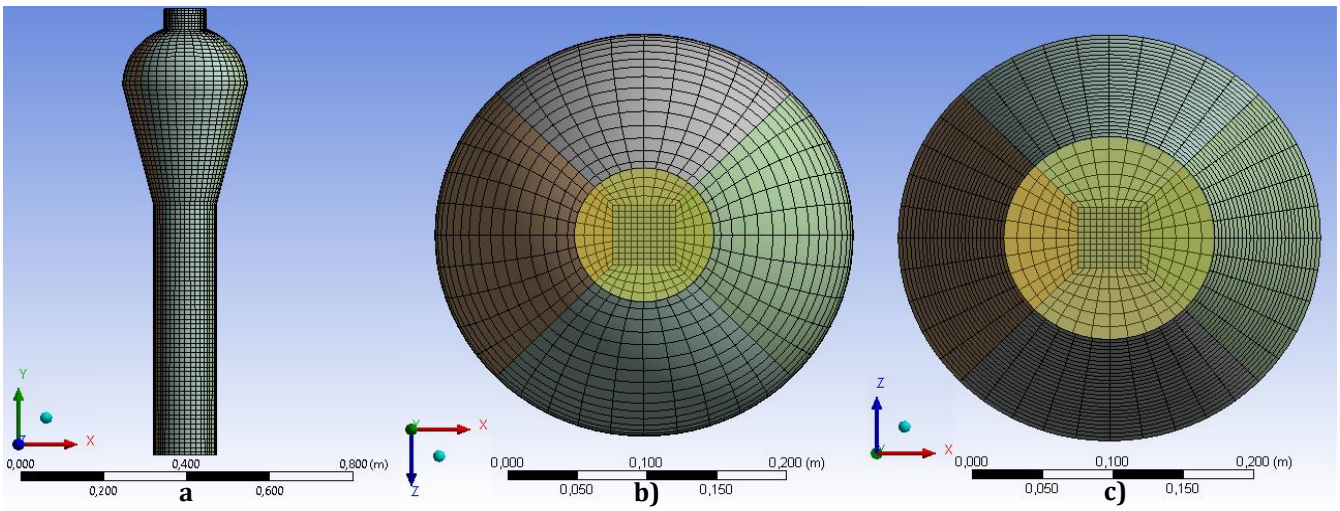

Figure 5- Mesh and boundary conditions for the pilot-scale fluidization unit with 118 557 nodes a) wall b) outlet c) inlet (CFD model simulation)

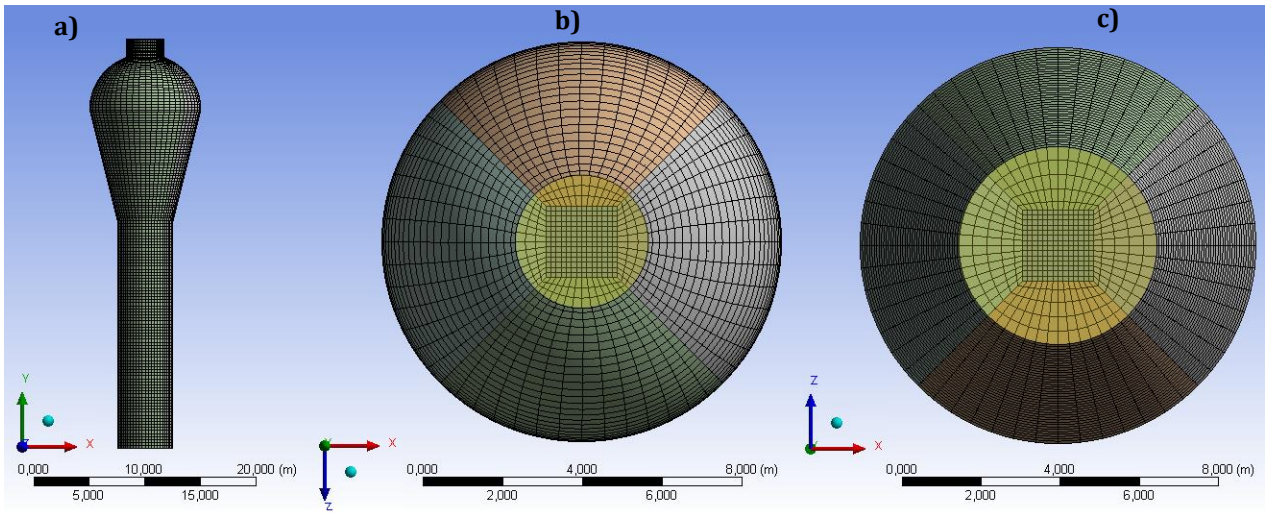

Figure 6-Mesh and boundary conditions for the industrial-scale reactor with 309 551 nodes a) wall b) outlet c) inlet (CFD-PBM simulation)

Table 4 - Kinetic parameters for CFD-PBM simulation in an industrial-scale FBR [15]

Kinetic parameter	Values
E_a , J/mol	33500
ΔH , kJ/mol	100
k_p^0 , m³/(mol·s)	$1 \cdot 10^{-6}$
Heat capacity, J/(kg· K)	2104
Thermal conductivity (W/(m· K)	0.084

Table 5- Boundary conditions and model parameters for CFD-PBM model simulation in an industrial-scale FBR

Description	Values
Granular viscosity	Gidspow
Granular bulk viscosity	Lun et al.
Frictional viscosity	Schaeffer
Angle of internal friction	30º
Granular temperature	Algebraic
Drag law	Gidspow
Coefficient of restitution for particle-particle collisions	0.9
Inlet boundary conditions	Velocity inlet
Outlet boundary conditions	Pressure outlet
Wall boundary conditions	No slip for air, specularity coefficient 0 for solid phase
Initial bed height	10
Initial volume fraction of solid phase	0.498
Operating pressure	2 MPa
Inlet gas velocity	0.38 m/s
Turbulent kinetic energy	0.000687 m^2/s^2
Turbulent dissipation rate	0.000128 m^2/s^3
Convergence criteria	0.01
Time step	0.01 s

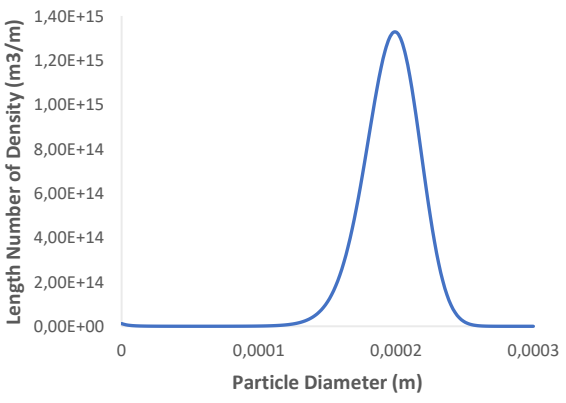

Figure 1- Initial particle size distribution for CFD-PBM model simulation in an industrial-scale FBR. [11]

The velocity used in the simulation was 3 u_{mf}, 0.38 m/s.

The initial particle size distribution used is shown in Figure 2.

3. EXPERIMENTAL METHODS

3.1 CDF MODEL VALIDATION

It is necessary to compare the particle flow behavior verified in the simulation with the experimental one, verified for the same velocity.

The simulation was performed for two different velocities, 3.3 m/s (Re=870), and 5.7 m/s (Re=1520). However, in the laboratory, particle flow behavior was recorded at three different velocities, 0.9 m/s, 3.3 m/s and 5.7 m/s.

The average pressure drop for experiment in Faculty's laboratory was 7 mbar, with an associated error of 18.85% compared to the theoretical value (5.89 mbar). The theoretical value was obtained from the classical equation (1) and (2).

From Figure 7 and Figure 9, the bed height can be observed along the particle bed in the y-axis. In both figures, it is possible to see a pattern in the particle flow behavior, and bed height is identical between the simulation and the laboratory's pilot-scale fluidization unit.

It is also possible to prove the fluidization regime, and there is a transition between the slugging fluidization and the turbulent fluidization for both situations. As expected, the bed height is higher in Figure 9, when the air velocity is higher.

It is possible to conclude that the developed model correctly predicts the particles' hydrodynamics.

Since the particles' hydrodynamics motion in an industrial-scale FBR is defined by the same computational models, and the CFD model has

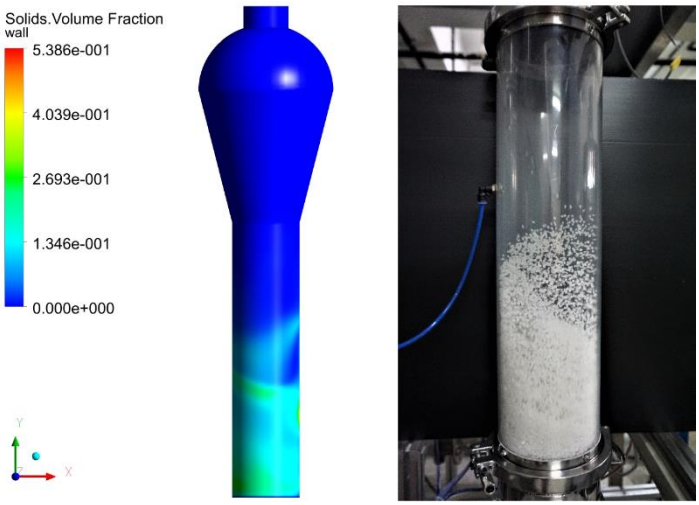

Figure 7 - Simulation results of particle flow behavior compared with experimental particle flow behavior in the laboratory's pilot-scale fluidization, both at 3.3 m/s.

been validated experimentally in the description of pilot-scale particle flow behavior, it is possible to apply the same CFD model in the industrial-scale FBR simulation.

Applying the CFD model to an industrial-scale FBR allows performing virtual experiments that are difficult to perform in the actual system. The CFD analysis is crucial for performing scale-up design since material costs prohibit iterative experimentation.

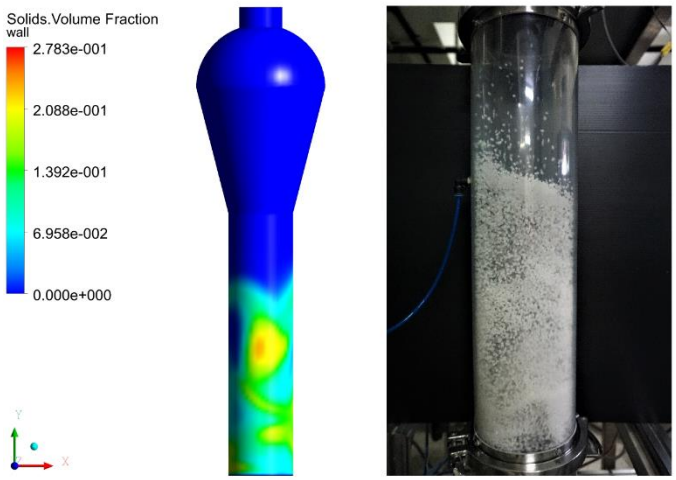

Figure 9 - Results of particle flow behavior compared with experimental particle flow behavior in the laboratory's pilot-scale fluidization unit, both at 5.7 m/s.

4. RESULTS

4.1 CFD-PBM COUPLED MODEL

The industrial-scale FBR was simulated with the 3D CFD-PBM model for about 250 s of real time simulation, to reach quasi steady state conditions. At the steady state fluidization condition, particles move vigorously inside the bed.

The u_{mf} is 0.38 m/s in order to fully and steadily fluidize the solid mixtures.

In the beginning, all the particles are stagnant since the velocity is lower than u_{mf}. With the increase of the gas velocity, the bed pressure drop steps up along the bed. Later, with the increasing of the gas velocity, the pressure drop decreases as small particles begin to fill the voids between coarse particles. Coarse particles remain unchanged.

Figure 10 shows the existence of two stages of flow regime with increasing gas velocity to show the sensitivity of the fluidization process to u_{mf}.

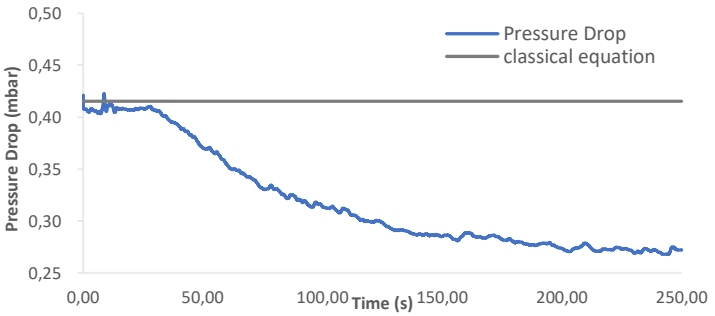

Figure 10 - Transient fluidization. Pressure drop in function of time in an industrial-scale FBR with a CFD-PBM simulation. Classical value of 0.4153 bar from classical equation (1) and (2).

First, from 0 to 30 s, the velocity is less than u_{mf}. The two initially well-mixed phases should not be separated. Thus, the particles remain in a fixed bed condition with nearly constant pressure drop (around 0.40 mbar) and void fraction, resulting in a homogeneous flow pattern. As the velocity increases, Figure 12, it starts to observe the fluidization of particles in a well-mixed condition, promoting contact between the catalyst particles with the monomer.

As the reaction begins, the particle size in the reactor increases. Considering the pressure drop equations (1) and (2), pressure loss could be expected to increase with the increasing volume fraction of solids. However, there is a decrease in pressure drop due to the decrease in particle fraction inside the reactor. Since the velocity chosen for the simulation is higher than the terminal velocity of the initial particles, they soon leave the reactor. About 30% of the initial solid was lost. This phenomenon is represented between 30 s and 210 s, shown in Figure 10. However, the pressure drop across the bed decreases to a constant value, which represents the fixed bed fluidization structure, 210s to 250s. Smaller particles have either left the reactor or have reached a sufficient size for fluidization.

During the simulation time, the superficial gas velocity gradually increases, as shown in Figure 12.

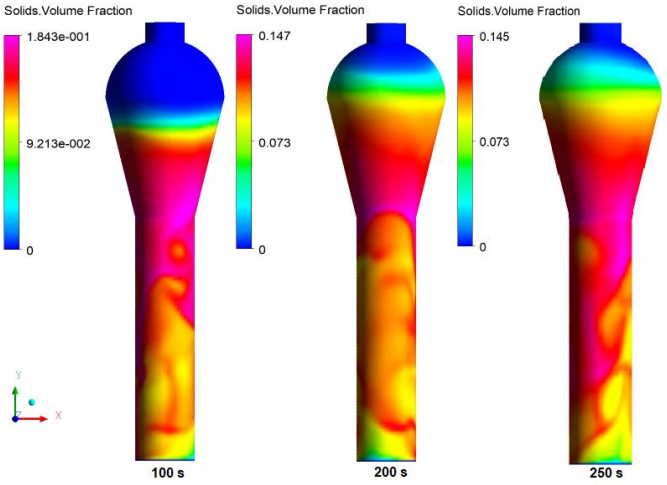

Figure 11 - The evolution of solid volume fraction contour in an industrial-scale FBR with a CFD-PBM simulation.

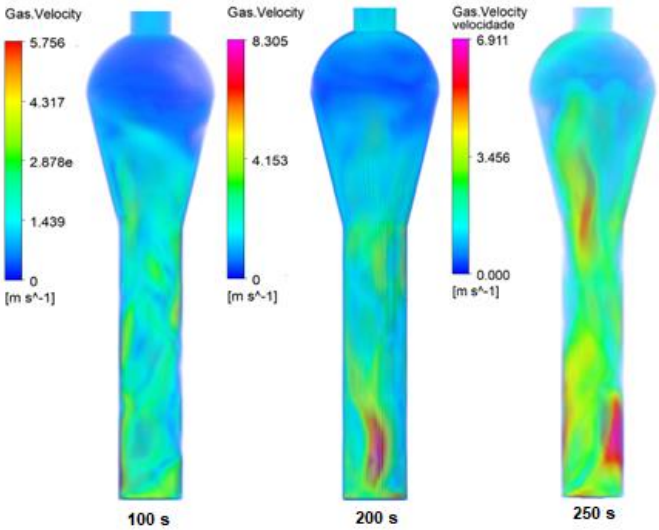

Figure 12- Volume rendering of gas velocity in an industrial-scale FBR with a CFD-PBM simulation.

In Figure 12, it is possible to verify that in the disengagement zone, the gas has a lower velocity. This decrease in velocity is due to the increased section area. In Figure 12 with Figure 11, it can be seen that along the reaction and freeboard zone, the gas has a higher velocity in the zones that have the smallest volume solids fraction. However, as the velocity increases, the fluidization regime changes.

Figure 13 shows the time-averaged solid velocities and volume fraction along the radial directions in the different heights inside the reactor.

In FBRs, it is quite common to find a typical flow structure consisting of two regions, the center-dilute core region, and the wall-dense annulus region. [18] The first one consists of a dilute upward-flowing suspension

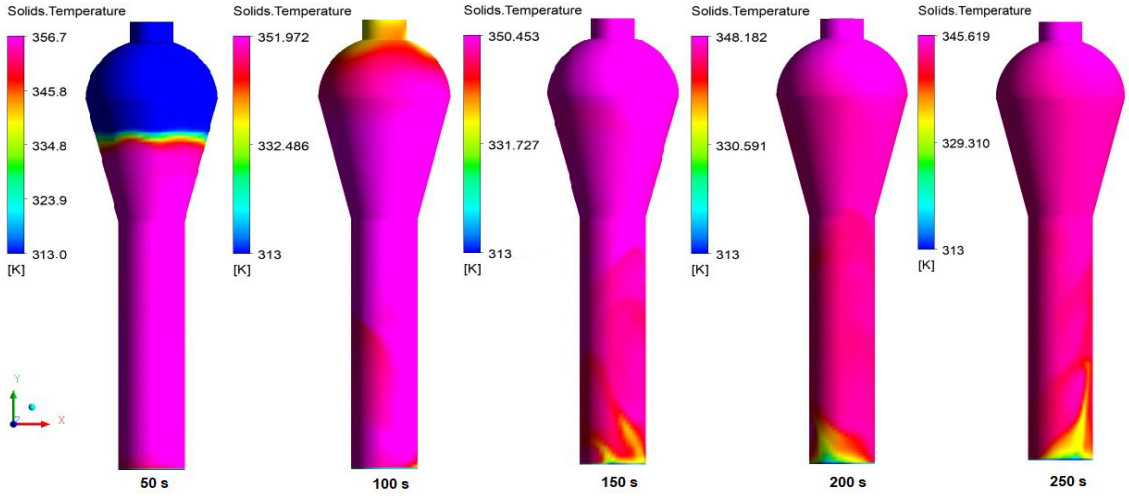

Figure 15 - The evolution of solids temperature contour in an industrial-scale FBR with a CFD-PBM simulation.

of solids, and the second one in the dense downward-flowing suspension of solids. Solid particle velocity and solid holdups can reveal these regions.

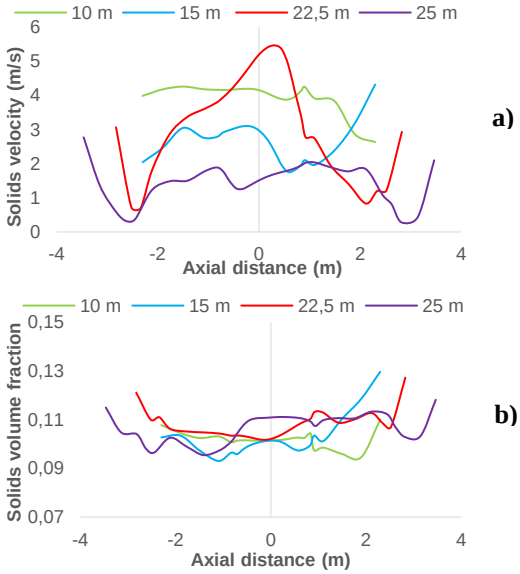

Figure 13 -The particle velocity profile along the radial direction (a) and the mean solid volume fraction along the radial direction(b) at 250 s in an industrial-scale FBR with a CFD-PBM simulation.

In Figure 13 b) can be seen a dilute-gas solid core in the center and a surrounding high solid volume fraction annular region near the wall.

Figure 13 a) shows the time-averaged axial particle velocity at each height of the vertical bed region. The particle velocity is inversely related to the solid volume fraction [16], as shown in $v_s = W_s/\rho_s\varepsilon_s$ where W_s is the solid flux (kg·m^{-3}·s^{-1}), ρ_s is solid density (kg·m^{-3}), and ε_s is the solid volume fraction. The higher the solid volume fraction, the lower the velocity.

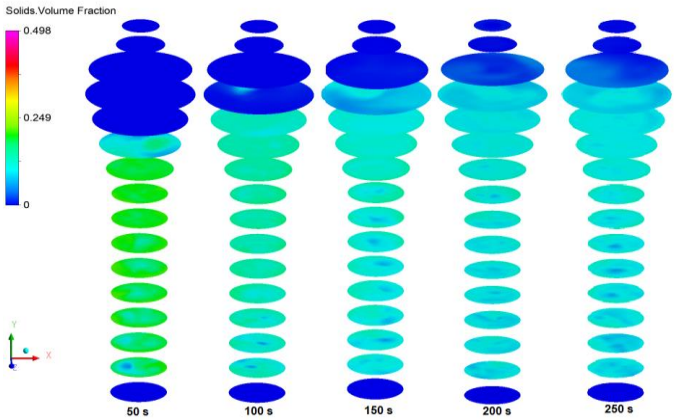

Figure 14- The evolution of solid volume fraction contour in the reactor for different heights in an industrial-scale FBR with a CFD-PBM simulation

Figure 14 shows that during the simulation, the central zone in the vertical section of the reactor bed has lower solid volume fraction values, which confirms what was said above. This accentuation of the distinction between the two regions over time is because it is approaching an ideal fluidization state.

As stated earlier, it is necessary to obtain a fundamental understanding of the temperature distribution in the bed since a temperature field can reflect the state of fluidization and helps verify the bed operating status. Since the ethylene polymerization reaction is extremely exothermic, it is necessary to remove the produced heat as quickly and efficiently as possible.

Figure 15 shows the mean temperature profiles for different simulation times. The industrial-scale FBR presents a non-uniform bed temperature. There is a temperature decrease within the reactor as the initial solids temperature set was 363k, and the gas temperature at the reactor inlet is 313K. The solids temperature gradually cools down.

Regarding particles size, the particle growth rate effect is considered because it is directly related to the polymerization kinetics. The particle size distribution is shown in term of the length number density, which represent the number of solid particles in the unit of volume of the reactor per unit particle diameter (m^3/m). The growth rate equation (56), is valid in the range of particle diameter $0 \leq L \leq 0.0012\ m$ [5].

In this dissertation, the mean particle diameter reached is 545.1 μm using the simulation time of 250 s, and an initial mean diameter of 200 μm. The average particle diameter as a function of time is shown in Figure 16.

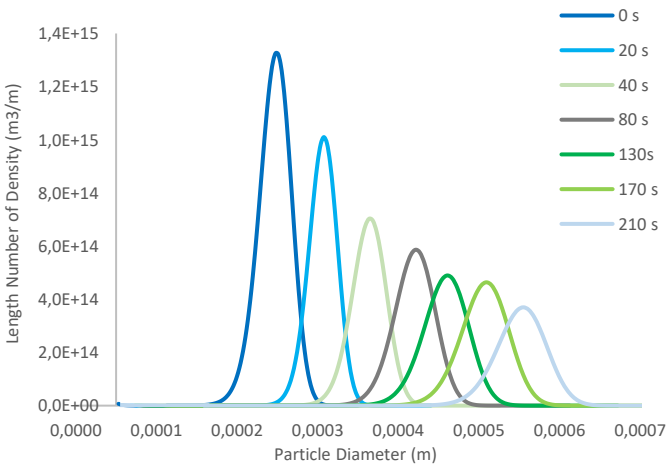

Figure 16 - The particle size distribution due to the growth rate in an industrial-scale FBR with a CFD-PBM simulation.

The particle growth rate of particles in the industrial-scale FBR is approximately $1.62\ \mu m/s$. The particle size progressively grows as the polymerization time increases. The particle distribution shows flatter as the particles grow due to more uniformity of particle size.

Based on equation (58), one can predict that the growth rate of smaller particles is faster than that of larger particles. With the

polymerization proceeding, the uniformity of particle sizes in the reactor increases and then the PSD gets broader. Therefore, the PBM coupled with the CFD model, can be used to describe the particle growth.

5. CONCLUSIONS

In this work, a 3D CDF-PBM couple model was developed to describe the gas-solid two-phase flow in an industrial-scale FBR, utilizing ANSYS Fluent software.

First, a 3D CFD model was developed to study the cold-flow behavior of PE particles in a pilot-scale fluidization unit. The 3D CFD model incorporates the Eulerian-Eulerian two-fluid model, KTGF, and turbulence model.

For the model validation, the pressure drop from the simulation results and the experimental pressure drop were compared with the pressure drop calculated through empirical equations, 5.89 mbar. The simulation and laboratory experiment were performed for two different velocities, $4u_{mf}$ =3.3 m/s (Re=870), and $7u_{mf} = 5.7\ m/s$ (Re=1520), during 6s real-time simulation. A pressure drop of 7 mbar and 5.91 mbar were obtained for the experimental and simulation results, respectively. There is an error of 0.34% for the simulation result, and 18.85% in the experimental result.

Although the simulation error to the theoretical value is practically nil, it is necessary to understand what may have affected the experiment since the error between the experimental and theoretical value is considerable. The device indicating the reactor pressure drop only shows the value of the units. Given the order of magnitude of the values concerned, this aspect has a significant influence on the result. Another aspect to be considered regarding the accuracy of the results is that the laboratory reactor is constantly opened and dismantled for experiments. Because of this, the sensors may be affected and influence the displayed value.

In the model validation, an analysis of the bed height can also be done. The flow behaviors were compared, verifying a transitional regime between slugging and turbulent, and the simulation results are consistent with the experimental data.

Subsequently, population balance, polymerization heat, and polymerization kinetics were incorporated into the validated model in order to develop a 3D CFD-PBM model for an industrial-scale FBR.

The 3D CFD-PBM coupled model was preliminarily tested by comparing the simulated results with the classical calculated data.

The simulation was performed for a velocity of $3u_{mf} = 0.38\ m/s$ (Re=769) during 30 s of real time simulation, obtaining a pressure drop of 0.4085 bar. Comparing this value with the value obtained through empirical equations, 0.4153 bar, an error of 1.65% is verified. Thus, the model can represent the actual behavior of real mixture with reasonable accuracy in terms of pressure drop.

Finally, the distinguished model was used to study the PE particle flow patterns and temperature field.

The results show that the pressure drop across the bed decreases to a constant value, which represents the fixed bed fluidization structure. In the first stage, the particles remain in a fixed bed condition with nearly constant pressure drop (around 0.40 mbar) and void fraction, resulting in a homogeneous flow pattern. As the velocity increases, it starts to observe the fluidization of particles in a well-mixed condition, promoting the reaction beginning. The particle size in the reactor increases, and the bed voidage also increases. As pressure drop is inversely related to void fraction, the pressure drop decreases.

The temperature of solid-phase increases from the bottom to the top of FBR since, in the disengagement zone, the convective heat transfer dominates the formation of temperature profiles in the growing particles. The simulated results also show that the inlet gas velocity is an essential factor in controlling the reactor temperature fields, verifying a decrease in reactor temperature over time. Thus, the industrial-scale FBR presents a non-uniform bed temperature.

Given the importance of the reactor temperature profile, several studies have been carried out to find a solution to improve this aspect. One option is to use rotating FBRs since that allows a uniform bed temperature [17]. However, this type of reactor is not yet used to produce PE at the industrial-scale.

The particle growth rate of the industrial scale FBR is approximately $1.62\ \mu m/s$, obtaining a final average particle diameter of $545.1\ \mu m$. However, in this work, the effect of aggregation and breakage was not considered. It was only considered the particle growth, adopting a kinetics model containing the mainly elementary chain propagation reaction. Thus, future work consists of the use of a comprehensive kinetic model, considering all the elementary reactions of PE polymerization process, species transport for gas and solid phase, and scalar transport. This will allow better accuracy regarding the PSD and flow behavior inside the reactor.

It is possible to conclude that the 3D CFD-PBM developed coupled model is not only appropriated to accurate simulate the flow behavior and PSD, but also brings together all the features presented in past articles applied on a 3D industrial-scale FBR. The 3D CFD-PBM model allows optimizing operating conditions and equipment design, leading to improved process safety and process efficiency, and decreasing capital and operating costs.

6. REFERENCES

[1] Ronca, S. (2016). Polyethylene. In Brydson's Plastics Materials: Eighth Edition. 10, 247- 277.

[2] Beroe Inc. (2018). Category intelligence on ethyl acetate.

[3] Patel, Rajen M. (2016). Polyethylene. In Multilayer Flexible Packaging: Second Edition. 2, 17- 34.

[4] Htu, T. C. M. (n.d.). Production of Polyethylene Using Gas Fluidized Bed Reactor. 1–20.

[5] Akbari, V., Nejad, T., Borhani, G., Shamiri, A., Kamaruddin, M., & Hamid, A. (2015). 2D CFD-PBM simulation of hydrodynamic and particle growth in an industrial gas phase fluidized bed polymerization reactor. In Chemical Engineering Research and Design (Vol. 104).

[6] Che, Y., Tian, Z., Liu, Z., Zhang, R., Gao, Y., Zou, E., … Liu, B. (2016). An Insight into the Temperature Field and Particle Flow Patterns in a Fluidized Bed Reactor for Nonpelletizing Polyethylene Process Using a 3D CFD-PBM Model. In Industrial and Engineering Chemistry Research (Vol. 55).

[7] Yao, Y., Su, J., & Luo, Z. (2015). CFD-PBM modeling polydisperse polymerization FBRs with simultaneous particle growth and aggregation : The effect of the method of moments. In Powder Technology (Vol. 272).

[8] J. B. P. Soares & T. F. L McKenna (2012). Polyolefin Reaction Engineering. Wiley-VCH.

[9] Yan, W., Luo, Z., Lu, Y., & Chen, X. (2012). PARTICLE TECHNOLOGY AND FLUIDIZATION A CFD-PBM-PMLM Integrated Model for the Gas – Solid Flow Fields in Fluidized Bed Polymerization Reactors (Vol. 58).

[10] Pan, H., Liang, X. F., & Luo, Z. H. (2016). CFD modeling of the gas–solid two-fluid flow in polyethylene FBRs: From traditional operation to super-condensed mode. Advanced Powder Technology, 27(4), 1494–1505.

[11] Yao, Y., He, Y. J., Luo, Z. H., & Shi, L. (2014). 3D CFD-PBM modeling of the gas-solid flow field in a polydisperse polymerization FBR: The effect of drag model. Advanced Powder Technology, 25(5)

[12] Chen, X. Z., Shi, D. P., Gao, X., & Luo, Z. H. (2011). A fundamental CFD study of the gas-solid flow field in fluidized bed polymerization reactors. Powder Technology, 205(1–3), 276–288

[13] C.K.K. Lun, S.B. Savage, D.J. Jeffrey, N. Chepurniy, (1984). Kinetic theories for granular flow-inelastic particles in Couette-flow and slightly inelastic particles in a general flow field, J. Fluid Mech. 140, 223-256.

[14] J. Ding, D. Gidspow, (1990). A bubbling fluidization model using kinetic-theory of granular flow, AIChE J. 36(4)

[15] Chen, X., Luo, Z., Yan, W., Lu, Y., & Ng, I. (2011). Three-Dimensional CFD-PBM Coupled Model of the Temperature Fields in Fluidized-Bed Polymerization Reactors (Vol. 57).

[16] Dfg - M. Kashyap, D. Gidaspow,W.J. Koves, (2011). Circulation of Geldart D type particles: part I —high solids fluxes. Measurements and computation under solids slugging conditions, Chem. Eng. Sci. 66, 183–206

[17] de Broqueville, A., & De Wilde, J. (2009). Numerical investigation of gas-solid heat transfer in rotating fluidized beds in a static geometry. Chemical Engineering Science, 64(6), 1232–1248.

[18] Che, Y., Tian, Z., Liu, Z., Zhang, R., Gao, Y., Zou, E., … Liu, B. (2015). A CFD-PBM model considering ethylene polymerization for the flow behaviors and particle size distribution of polyethylene in a pilot-plant fluidized bed reactor. Powder Technology, 286, 107–123.